Copy
RM E58A27

4

NACA RM E58A27

C2

NACA

RESEARCH MEMORANDUM

INVESTIGATION OF TWO-STAGE COUNTERROTATING COMPRESSOR IV - OVER-ALL PERFORMANCE OF COMPRESSOR WITH MODIFIED SECOND-STAGE ROTOR

By Ward W. Wilcox and William Stevans

Lewis Flight Propulsion Laboratory
Cleveland, Ohio

NATIONAL ADVISORY COMMITTEE
FOR AERONAUTICS

WASHINGTON
May 20, 1958

NACA RM E58A27

NATIONAL ADVISORY COMMITTEE FOR AERONAUTICS

RESEARCH MEMORANDUM

INVESTIGATION OF TWO-STAGE COUNTERROTATING COMPRESSOR IV - OVER-ALL PERFORMANCE OF COMPRESSOR WITH MODIFIED SECOND-STAGE ROTOR

By Ward W. Wilcox and William Stevans

SUMMARY

Preliminary tests of a counterrotating axial-flow supersonic compressor indicated that a flow limitation in the second rotor restricted the flow rate at design speed. In an effort to increase the flow rate and improve flow stability, the second-stage rotor was modified by increasing the flow area. The flow rate and the stability were both improved somewhat, and a wide variety of combinations of first- and second-stage speeds was possible. With the first rotor at a tip speed of 1260 feet per second (design) and the second stage at 1318 feet per second (110-percent design), a pressure ratio of 4.51 was obtained at a weight flow rate of 28.15 pounds per second per square foot frontal area and an adiabatic efficiency of 0.71.

INTRODUCTION

A counterrotating axial-flow supersonic compressor was designed, constructed, and tested as discussed in references 1 to 3. As noted in reference 3, the preliminary tests of the complete unit indicated that a flow limitation within the second rotor restricted the flow rate at design speed. In addition, at speeds below design, this flow limitation forced the first rotor to operate in a region where stalling had occurred when the first stage was tested alone. An effort was made to remove this flow limitation and to improve the flow stability by modifying the flow-area distribution within the second rotor and in the outlet annulus.

The results of the modifications are presented in this report, along with more complete over-all performance data than that presented in reference 3. Sufficient data are presented to allow compressor -turbine matching studies to be made.

SYMBOLS

A_F	frontal area of first rotor, sq ft
H	total enthalpy
i	incidence angle
M	Mach number
N	rotational speed, rpm
P	total pressure
r	radius, in.
ωr	rotor speed, ft/sec
T	total temperature, $^{\circ}R$
w	weight flow, lb/sec
β	flow angle with axis of rotation, deg
δ	ratio of inlet pressure to NACA standard sea-level pressure of 2116.2 lb/sq ft
η_{ad}	adiabatic efficiency
θ	ratio of inlet temperature to NACA standard sea-level temperature of 518.7° R

Subscripts:

t	tip
0	compressor inlet
1	first-rotor inlet
2	first-rotor outlet
2a	second-rotor inlet
3	second-rotor outlet

Superscript:

'	relative to rotor

APPARATUS

The compressor test rig was basically unchanged from the rig discussed in references 1 and 3 except for modifications to the second rotor and the fairing behind it. The schematic sketch of figure 1 gives an over-all view of arrangements within the test rig. Table I lists the important design parameters.

Modifications to Second Rotor

As mentioned briefly in reference 3, the axial area distribution through this rotor was not exactly as designed because of errors in the hub profile. As a rather crude approximation, the area was determined from the product of the annulus area and the cosine of the flow angle less the actual blade cross-sectional area at each station. In computing this area distribution from the blades as designed, the pitch-line angle distribution was used as being applicable at all radii. This area distribution is given by the solid line in figure 2.

A desirable method of "opening up" the second-stage rotor would be to decrease the hub diameter without altering the blade profiles. However, because of the thin platforms used on this blade base, only a limited change could be made in the hub. The modified hub contour is shown by the dashed line of figure 3. Accordingly, some metal was removed from the blade profiles, as shown by the thickness distribution curve of figure 4. The net result of these alterations (calculated by the method just given) is shown by the dashed line in figure 2.

Modification to Rear Fairing

A new inner rear fairing was constructed for tests of the modified rotor. The maximum diameter matched the rotor hub at the outlet, and a 2° taper of the inner wall was included for flow stability in the annulus.

RESULTS AND DISCUSSION

Over-All Performance of Modified Compressor

Change in weight flow. - Although the obtainable area increase was restricted by mechanical limitations of the second rotor, some improvement was noted in weight flow capacity. Figure 5 shows the maximum inlet equivalent weight flow for the original (ref. 3) and the modified compressors at the various speed combinations. In general, the increase in weight flow at all first-stage speeds confirms the belief that the flow limitation was originally in the relative flow within the second rotor.

At design speed, the maximum equivalent weight flow was increased from 27.20 pounds per second per square foot to 28.5 pounds per second per square foot.

For speed combinations where the second-stage speed was greater than the first, the operation was in the stall-free range as determined in the single-rotor tests of reference 1. With both rotors operating at the same speed, the maximum flow point for the modified combination was also within the stall-free range. This margin was small at most speeds, however, and actual stalling did occur at lower weight flows. In general, the stall pulses were irregular and relatively mild, rather than periodic. For a better stall margin on the first rotor while maintaining a reasonable pressure ratio, a match point in the region of 29.8 pounds per second per square foot would be desirable. To achieve operation at this point, a further increase of the same magnitude would be required in the second-stage flow area.

In all these tests, the weight flow limit was set by the second rotor, and the limiting weight flow of the first rotor was not reached. At most speed combinations, the range of weight flows was greater for the modified rotor than for the original configuration.

Pressure ratio. - In figure 6, the over-all mass-weighted average pressure ratio is plotted against specific equivalent weight flow for all speed combinations tested. Data from the original configuration have been included as tailed symbols for comparison. In the low- and medium-speed ranges, pressure ratio for the modified compressor is not consistently higher or lower than for the original configuration, but the weight flow is higher at all speeds. At design speed, the majority of data indicate a lower pressure ratio with the modified rotor, although the data points exhibit considerable scatter.

A possible operating point where blade stresses would be reasonably low might be selected at the 100-percent first-stage, 110-percent second-stage speed configuration. At this operating condition a pressure ratio of 4.51 was obtained at a weight flow of 28.15 feet per second per square foot, and an adiabatic efficiency of 0.71. Further, the outlet absolute Mach number was about 1.0, which is rather low for supersonic compressors.

Efficiency. - The over-all adiabatic efficiency is shown in figure 7. A large amount of scatter existed in the adiabatic efficiency data, but some trends are evident. For the range of weight flows covered, with two-stage operation the efficiency of the first stage improves with increasing weight flow. As a result, the over-all efficiency at a given speed combination increases with weight flow. When first-stage speed is held constant and second-stage speed is increased, the second-stage inlet Mach number increases, and second-stage efficiency is reduced. This effect counteracts the improvement in first-stage efficiency due to increasing

weight flow. However, as the speed of either the first or second stage is increased, the over-all efficiency level decreases because the second-stage losses are increasing. In all cases, the second stage supplies the greater part of the energy addition and has the greater influence on efficiency. At the higher speeds, the open throttle point has an artificially high efficiency because the normal shock loss has not been charged to the pressure ratio. To distinguish these points, a tail has been added to the symbol in the figure whenever the outlet Mach number exceeds 1.4.

4655

Radial Variation of Flow Conditions and Performance Parameters in Second Rotor

Figure 8 gives the radial variation of second-stage pressure ratio, temperature-rise ratio, and adiabatic efficiency for first-stage tip speeds varying from 50- to 110-percent design with the second-rotor speed held constant at 100 percent. In all cases, the speeds were determined as the percent equivalent speeds, based on the first-stage inlet temperature. To use second-stage inlet temperature for setting the second-stage equivalent speed would require a method of integrating the radial variation in temperature in a very short time. The operating points given in figure 8 are at or near peak efficiency operation. The radial variations shown are not as great as were found with the first rotor.

Despite the fact that the second-stage energy addition shown by the temperature-rise ratio is lowest at the 50-percent first-stage speed, the second-stage pressure ratio is highest as a result of the good adiabatic efficiency. For the operating points presented in figure 8, the actual equivalent speed of the second rotor, computed from average between-rotor temperatures, varied from 108.9 to 97.4 percent of design as the equivalent speed of the first rotor was increased from 50 to 110 percent of design. As a result, the indicated second-rotor energy addition (fig. 8(b)) is higher at low first-rotor speeds and lower at high first-rotor speed than would be expected if the real equivalent speed of the second rotor had been maintained constant. In any case, reference to the design second-rotor energy addition (indicated by dashed line in fig. 8(b)) shows that the actual energy addition was below design at most operating conditions at or near design speed.

In figure 9, flow conditions relative to the second-stage rotor blades are given as variations with radius for the same compressor operating points presented in figure 8. In figure 9(a), which gives the radial variation of incidence angle, the incidence at first-stage speed from 50 to 80 percent varies only slightly with radius or speed. At the higher speeds (90 to 110), the incidence angle is nearly zero near the hub and reaches higher values near the outer wall.

As shown in figure 9(b), the radial distribution of inlet relative Mach number was very uniform at all first-stage speeds. However, for each first-stage speed, there is a characteristic Mach number plateau that increases rapidly with first-stage speed.

The radial variation of total-pressure recovery factor (ratio of relative total pressure to ideal relative total pressure at outlet) corresponding to the two previous figures is given in figure 9(c); this figure shows that pressure recovery decreases consistently with increasing inlet relative Mach number. Near the hub, nearly every increase in Mach number is accompanied by a decrease in pressure recovery. However, near the tip, some inconsistencies may be seen at high speeds; these might be the result of the changes in incidence angle. In general, the level of pressure recovery is considerably below the normal shock recovery at the equivalent Mach number.

Stability of Shock Wave in Second Rotor

In unstarted supersonic rotors such as the second-stage rotor discussed herein, a shock configuration usually exists external to the passage minimum area. Conditions downstream of the shock depend on back pressure; that is, for low pressure a supersonic expansion exists, and for high back pressures completely subsonic flow exists. During application of back pressure (by throttling downstream), a normal shock wave is forced upstream and eventually merges with the external shock.

In the original configuration of the counterrotating compressor, stabilization of the second normal shock in the second-stage rotor passage was impossible. As back pressure was applied, the shock moved forward through the annulus to the rear of the compressor. Further application of back pressure moved the normal shock into the rotor briefly; but, with any small disturbance of flow, the shock jumped through the rotor and surging resulted. Figure 2 shows that, when the rotor modification was made, the minimum area location was shifted forward by approximately 1/2 inch. As a result, a longer divergence section was obtained in the modified rotor; this tended to stabilize the second shock.

Figure 10 shows the ratio of wall static pressure to inlet tank pressure plotted against axial distance at design speed for the original configuration from reference 3. Superimposed on this figure is the corresponding plot for the modified impeller with back pressure applied. At this operating point, there is no reacceleration within the rotor passage, and no surging occurs. In figure 11(a), the ratio of outer-wall static pressure to inlet total pressure is plotted against axial distance for even-speed combinations. These curves show the presence of an external shock system in the forward part of the second-rotor blade channel. In the rear part of the channel, with low back pressure, the flow expands

supersonically to Mach numbers determined by the air collection system. This figure also shows that the external shock system moves farther into the channel as the speed (and second-stage inlet relative Mach number) increases.

Similar plots, given in figure 11(b), show the casing pressure ratios when back pressure has been applied. In this instance the second shock has been moved forward to merge with the external shock configuration, and little or no expansion occurs in the rear of the blade. In addition, the position of the initial shock configuration also has been moved forward. At most speed combinations, it was possible to operate over a range of second shock positions with varying back pressure.

In figure 12, casing pressure profiles are given for the high-back-pressure condition where the second-stage speed is held constant at 100 percent and the first-stage speed is varied from 50 to 110 percent. In general, these plots are much the same as for the even-speed case, although the variation in peak pressure is less. These plots indicate that the second-stage static-pressure rise is dependent largely on inlet relative Mach number rather than tip speed.

Individual Stage Performance

For application to jet engines, no compressor is entirely satisfactory unless it can be matched to the driving turbine properly. In the case of the counterrotating compressor, the obvious construction is of the two-spool type with separate turbines for inner and outer spools. An analytical study of the turbines for this application is reported in reference 4. Two-spool matching procedures are reported in reference 5. According to present indications, no matching study of this counterrotating compressor will be made. In addition to the performance parameters already discussed, second-stage pressure ratio and energy addition at constant percentages of design speed are plotted against specific equivalent weight flow, in order to allow a matching study to be made.

The characteristic map of first-stage performance is given in reference 1. For convenience the first-stage energy addition against inlet weight flow is plotted in figure 13. The second-stage energy addition is given in figure 14 for the range of speed combinations covered; from this figure, the dependence of second-stage energy addition on first-stage prerotation may be seen. For instance, at a constant second-stage speed of 100 percent, the peak energy addition increases from 42.5 to 55 Btu per pound as the first-stage speed is increased from 50 to 100 percent. However, as discussed previously, the equivalent tip speed of the second rotor is actually decreasing because of the increasing energy addition of the first stage. At a given weight flow, a wide choice of second-stage energy addition is available by choice of speed combinations. Comparison

of figures 13 and 14 shows that the change of energy addition with weight flow at a given speed combination is much greater for the second stage. This characteristic results from the changing flow condition at both inlet and outlet of the second rotor.

In figure 15, the second-stage pressure ratio is plotted against inlet weight flow. In contrast to the behavior of the energy addition, the pressure ratio is relatively constant with weight flow and first-stage speed. At the higher speeds, there is some decrease in second-stage pressure ratio as first-stage speed increases, despite the increasing energy addition shown in figure 14. This trend is largely a result of increased losses as the inlet relative Mach number increases.

4655

SUMMARY OF RESULTS

Tests of the modified version of the counterrotating supersonic compressor have shown:

1. A major improvement in stability of the shock wave system occurs in the second rotor at high back pressure. As a result of improved stability, some range of weight flow exists even at high speeds.

2. There is some improvement in weight flow capacity of the second rotor, with better matching between the first- and second-stage weight flow capacity. Physical limitations of rotor construction prevented further opening up of the second rotor.

3. The first rotor can be operated entirely out of the rotating stall region with the rotors at even speeds. However, operation in the region where the first rotor had rotating stall when tested alone was accomplished without periodic stall pulses.

4. A pressure ratio of 4.51 was obtained at a weight flow of 28.15 pounds per second per square foot frontal area and an adiabatic efficiency of 0.71. For this operation, the first rotor was operated at 1260 feet per second (100-percent design), and the second rotor at 1318 feet per second (110-percent design). At this operating condition, the outlet absolute Mach number was about 1.0.

Lewis Flight Propulsion Laboratory
National Advisory Committee for Aeronautics
Cleveland, Ohio, February 10, 1958

REFERENCES

1. Wilcox, Ward W., and Wright, Linwood C.: Investigation of Two-Stage Counterrotating Compressor. I - Design and Over-All Performance of Transonic First Compressor Stage. NACA RM E56C15, 1956.

2. Wright, Linwood C., and Wilcox, Ward W.: Investigation of Two-Stage Counterrotating Compressor. II - First-Rotor Blade-Element Performance. NACA RM E56G09, 1956.

3. Wilcox, Ward W., and Wright, Linwood C.: Investigation of Two-Stage Counterrotating Compressor. III - Design of Second-Stage Rotor and Preliminary Over-All Performance. NACA RM E56G30a, 1956.

4. Stewart, Warner L.: Investigation of Rotating Components of Counterrotating Two-Spool Engines. I - Analytical Investigation of Off-Design Performance of Turbine Component Designed With and Without Outer-Turbine Stator. NACA RM E54J13, 1955.

5. Dugan, James F., Jr.: Two-Spool Matching Procedures and Equilibrium Characteristics of a Two-Spool Turbojet Engine. NACA RM E54F09, 1954.

TABLE I. - DESIGN VECTOR DIAGRAMS FOR COUNTERROTATING COMPRESSOR

[Design speed, 18,030 rpm; r_t, 8.0 in.]

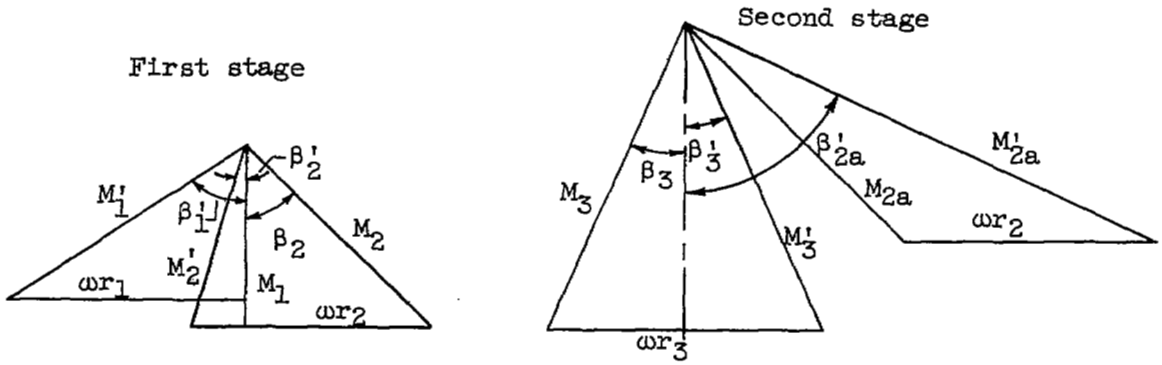

	Hub	Mean	Tip
% Flow	100	50	0
M_1	0.572	0.636	0.567
M_1'	.801	1.12	1.29
M_2'	.678	.727	.686
M_2	1.045	.955	.734
β_1'	45.5°	55.4°	63.94°
β_2'	-16.65°	17.76°	44.2°
β_2	53.58°	43.8°	47.15°
r_1/r_t	.500	.786	.996
r_2/r_t	.611	.807	.953
T_2/T_1	1.243	1.243	1.243
P_2/P_1	1.92	2.10	1.72

	Hub	Mean	Tip
% Flow	100	50	0
M_{2a}	1.24	1.04	0.777
M_{2a}'	1.83	1.76	1.66
M_3'	.983	1.14	.80
M_3	1.13	1.13	1.15
β_{2a}'	61.91°	63.15°	70.36°
β_3'	11.96°	23.01°	24.84°
β_3	31.75°	22.2°	37.6°
r_2/r_t	.64	.81	.95
r_3/r_t	.828	.89	.95
T_3/T_2	1.412	1.358	1.428
P_3/P_2	2.71	2.65	2.5

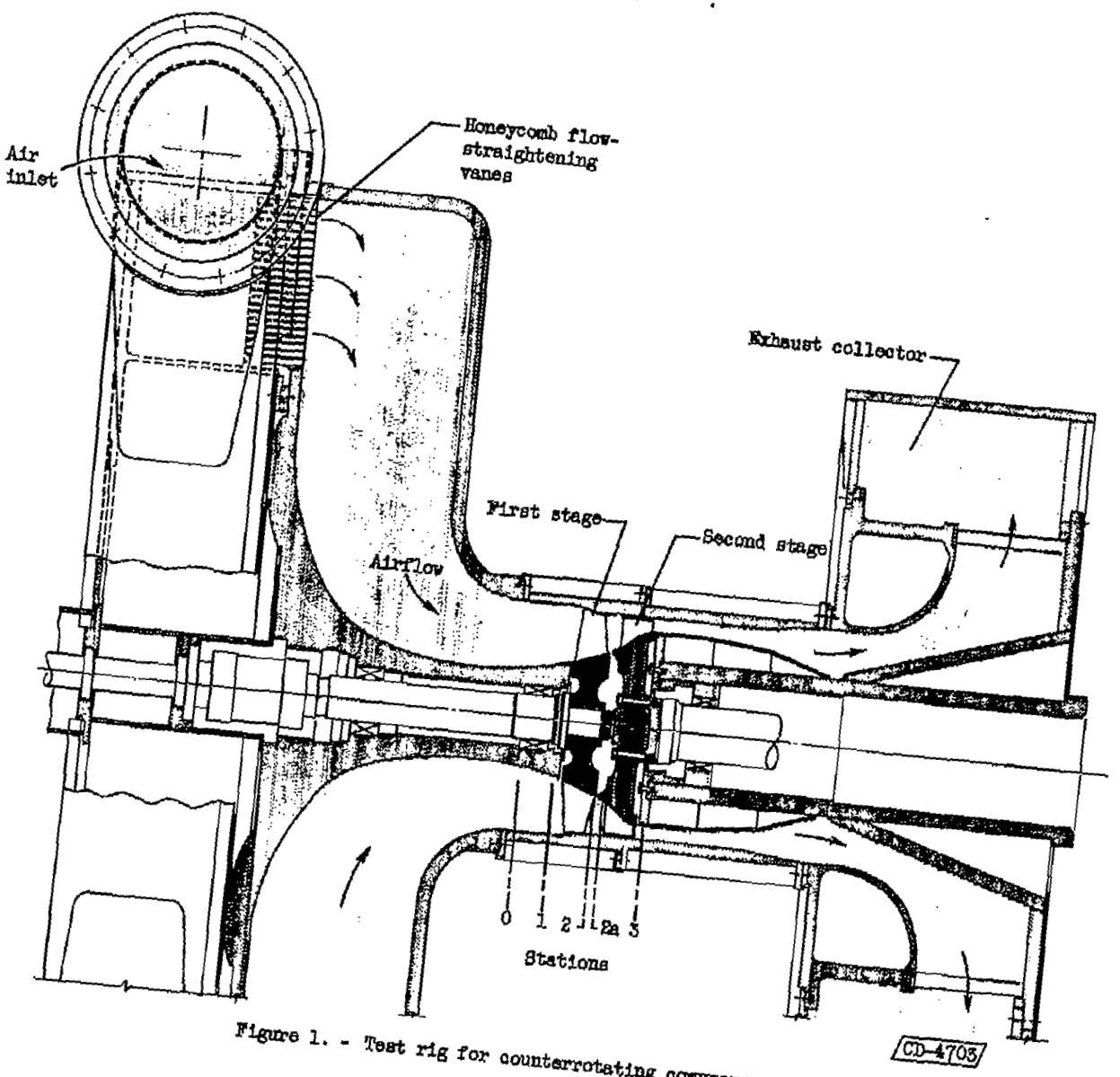

Figure 1. - Test rig for counterrotating compressor.

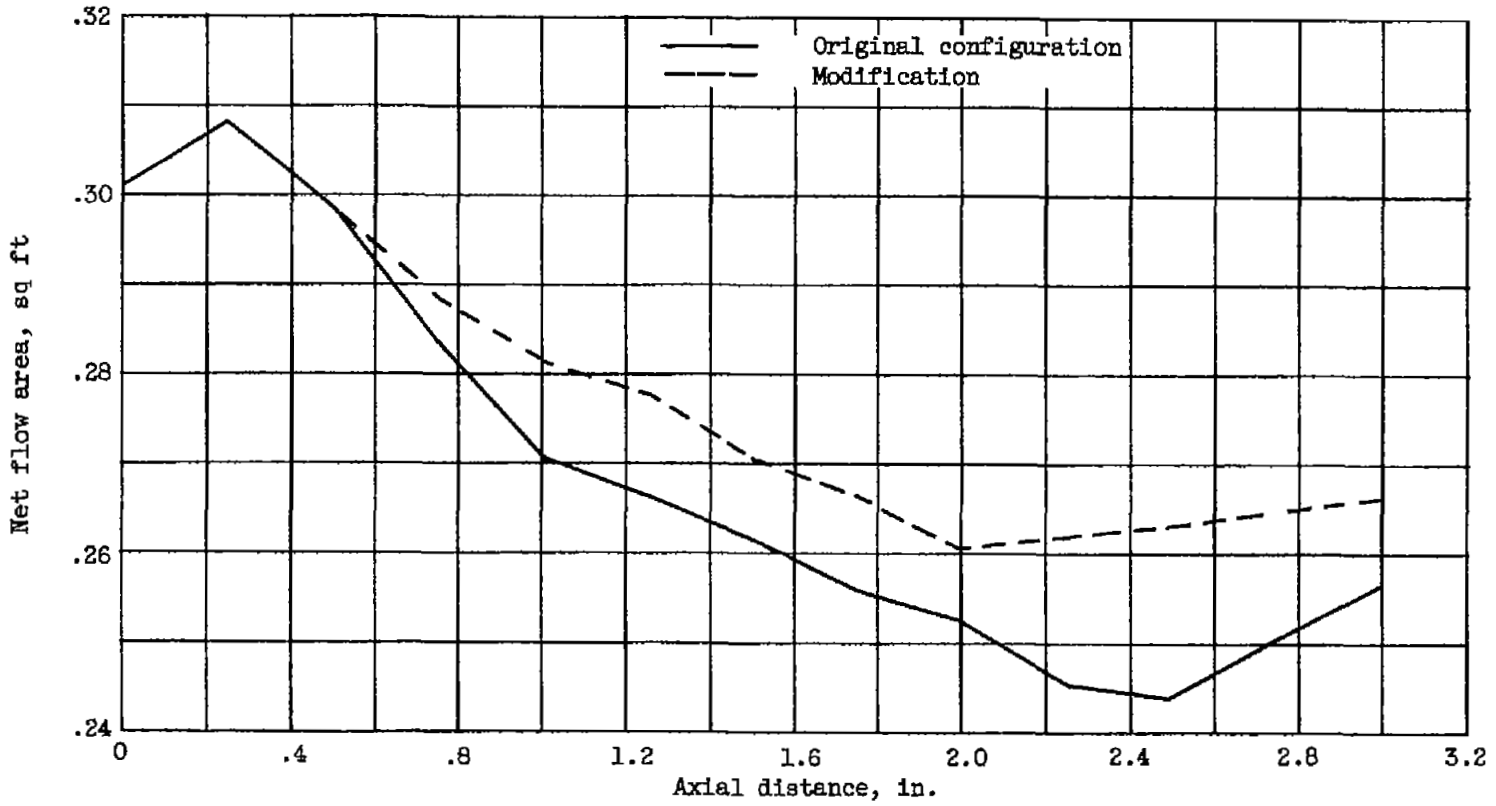

Figure 2. - Distribution of flow area through original and modified second-stage rotor.

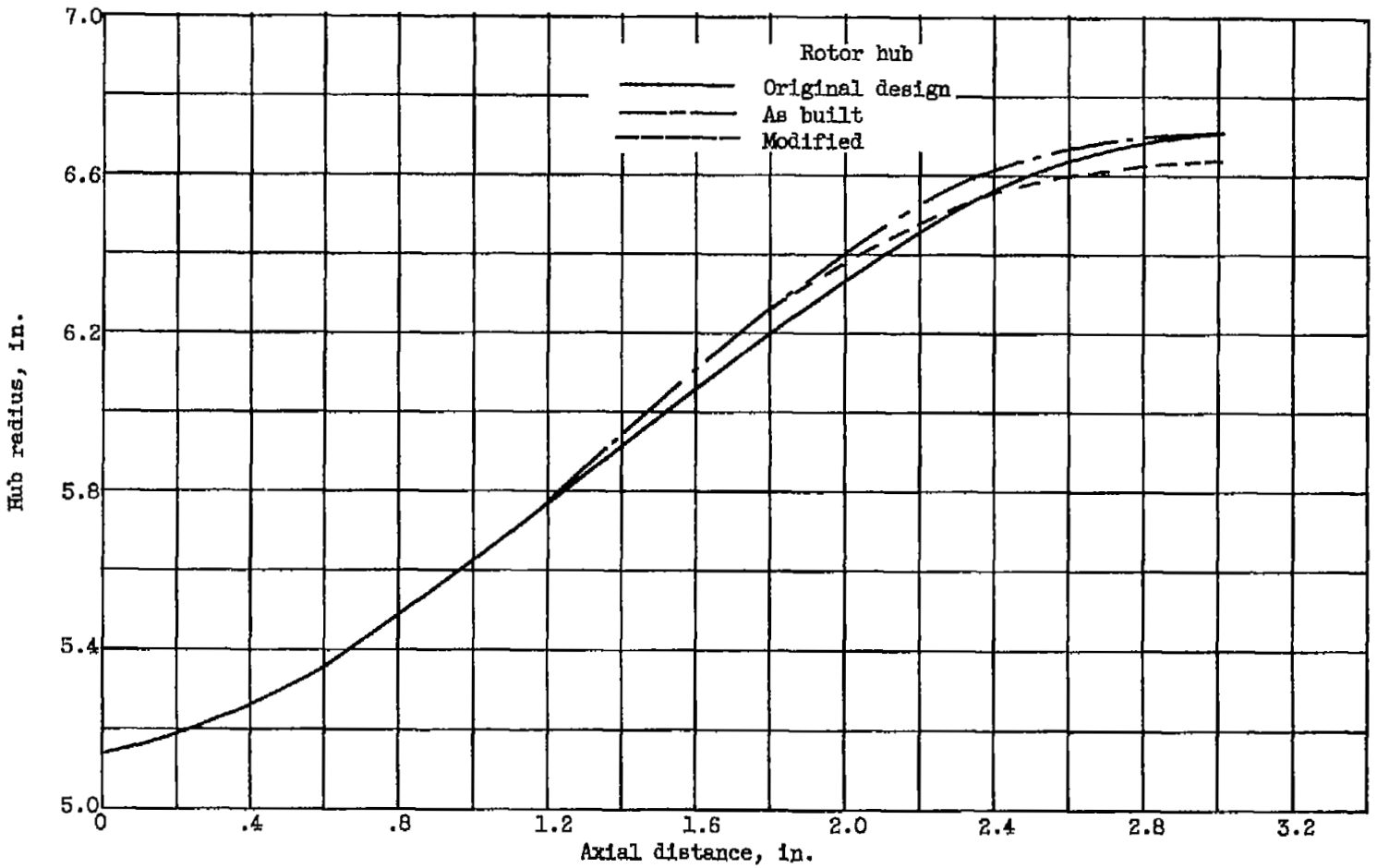

Figure 3. - Comparison of rotor hub contours.

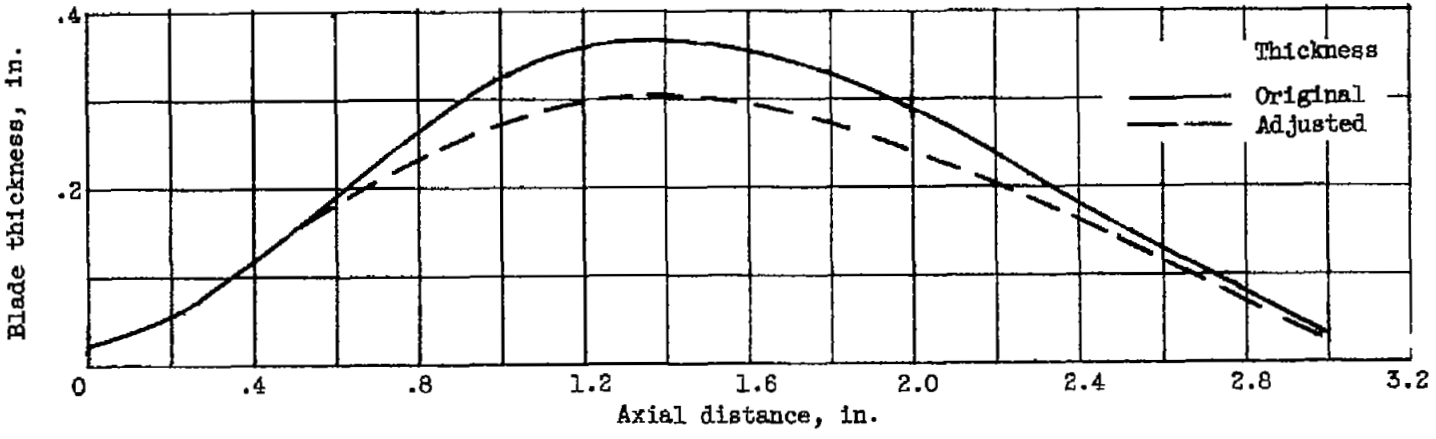

Figure 4. - Original and modified thickness distribution.

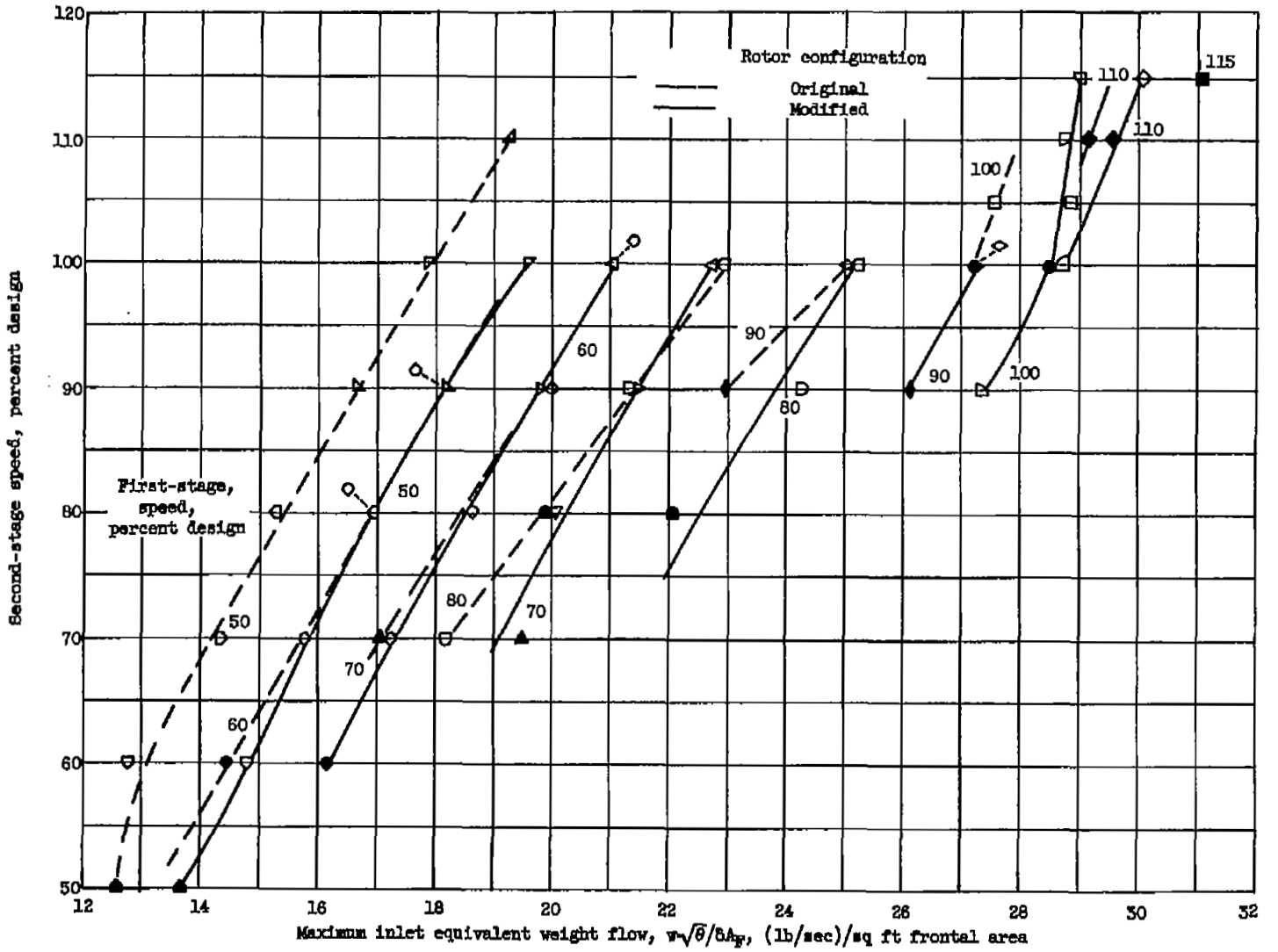

Figure 5. - Maximum specific equivalent weight flow for original and modified counterrotating compressors.

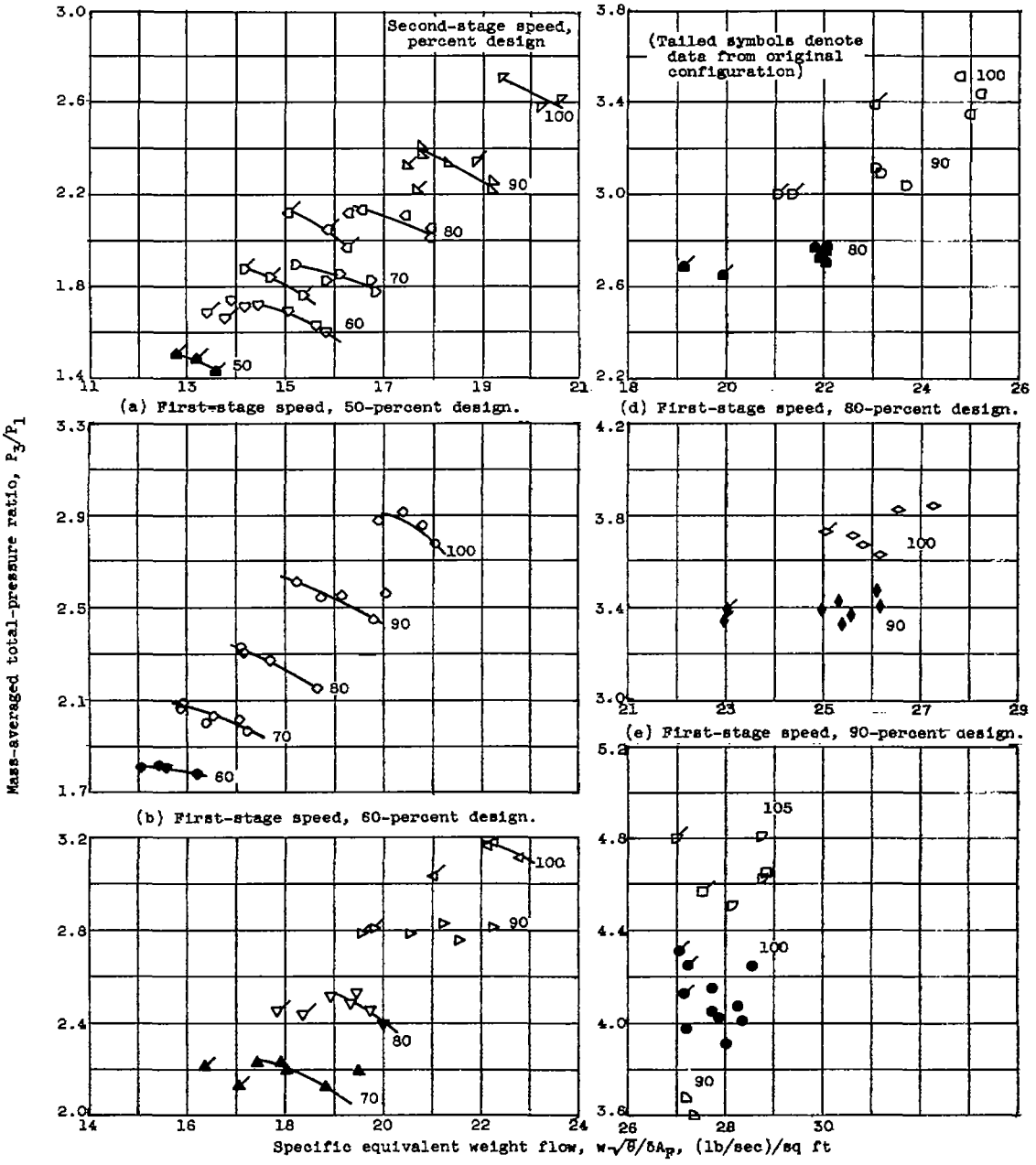

Figure 6. - Over-all pressure ratio of counterrotating compressor at various speed combinations.

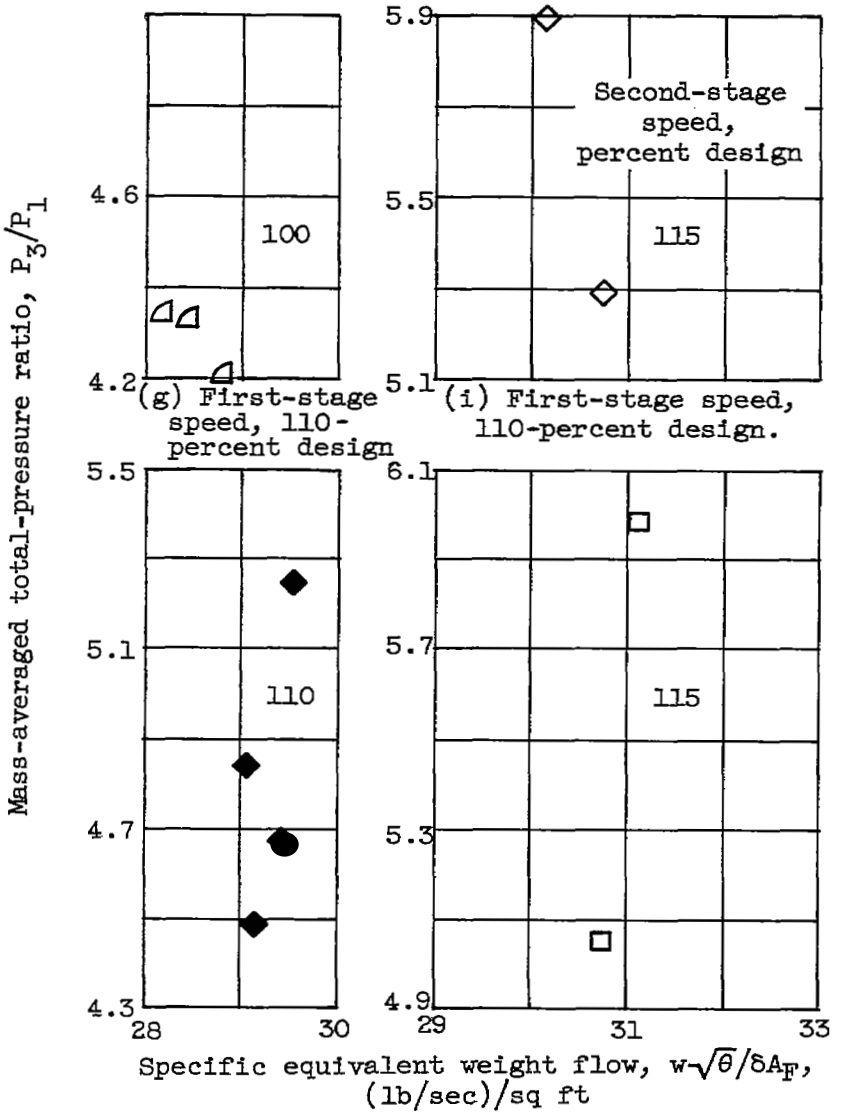

(g) First-stage speed, 110-percent design

(i) First-stage speed, 110-percent design.

(h) First-stage speed, 110 percent design.

(j) First-stage speed, 115-percent design.

Figure 6. - Concluded. Over-all pressure ratio of counterrotating compressor at various speed combinations.

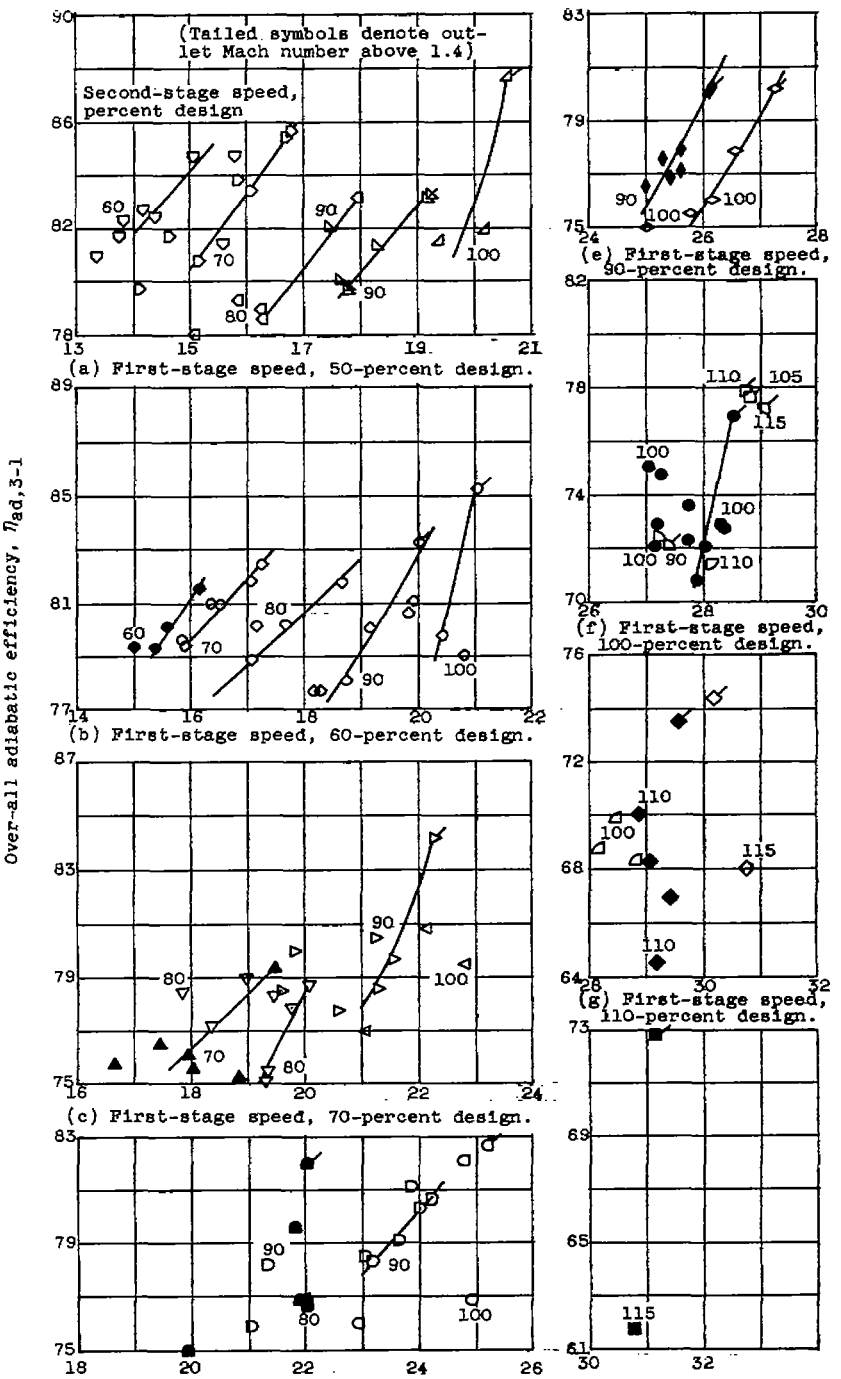

Figure 7. - Over-all adiabatic efficiency of counterrotating compressor at various speed combinations.

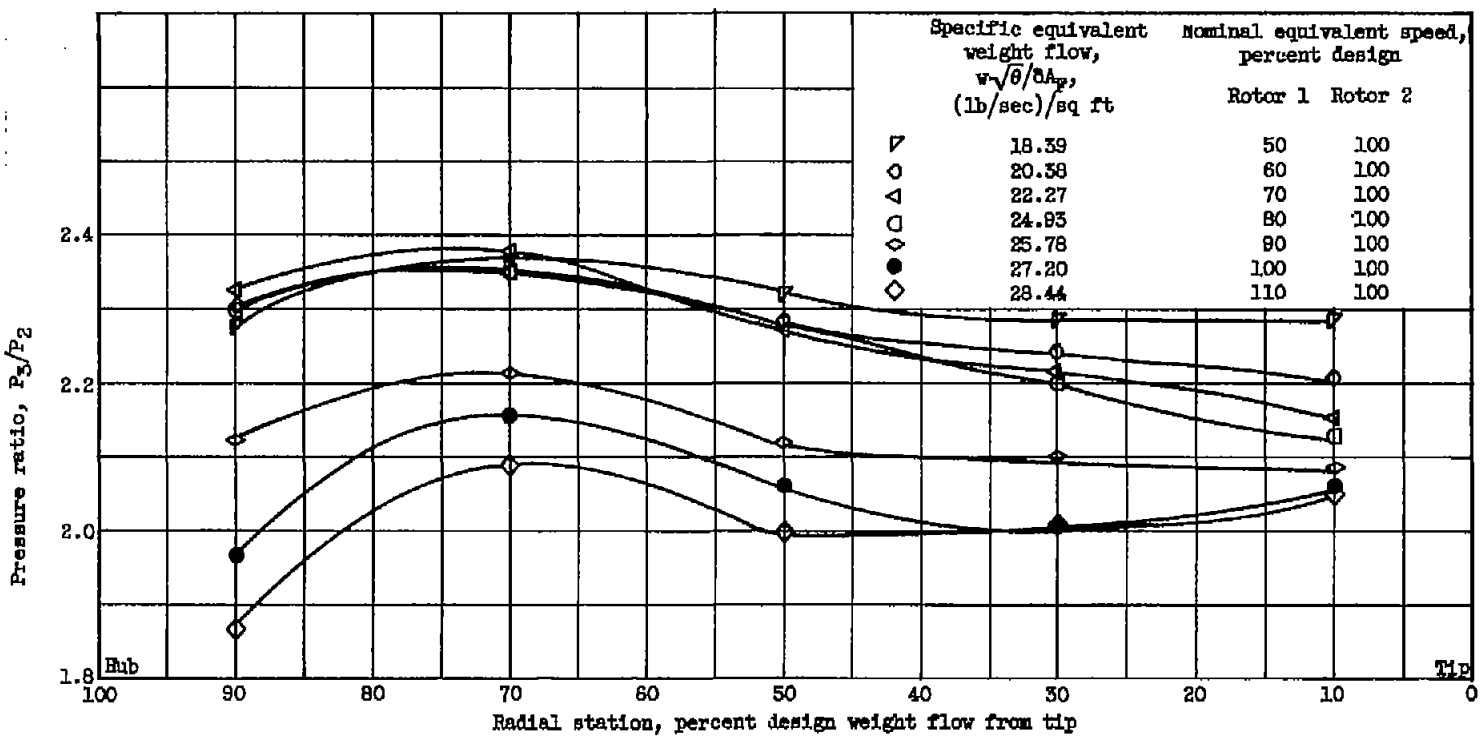

(a) Pressure ratio.

Figure 8. - Radial variation of second-stage performance.

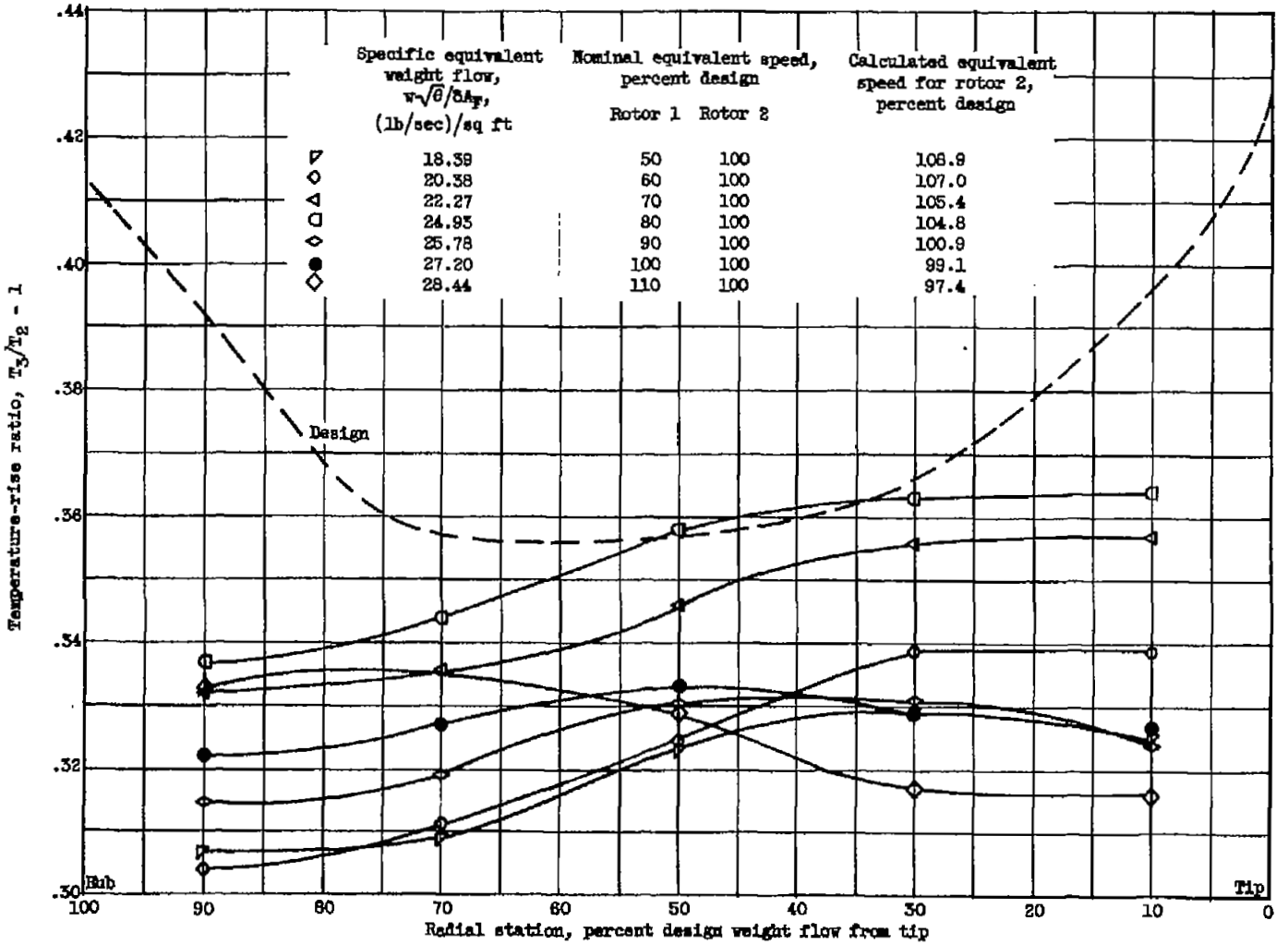

(b) Temperature-rise ratio.

Figure 8. - Continued. Radial variation of second-stage performance.

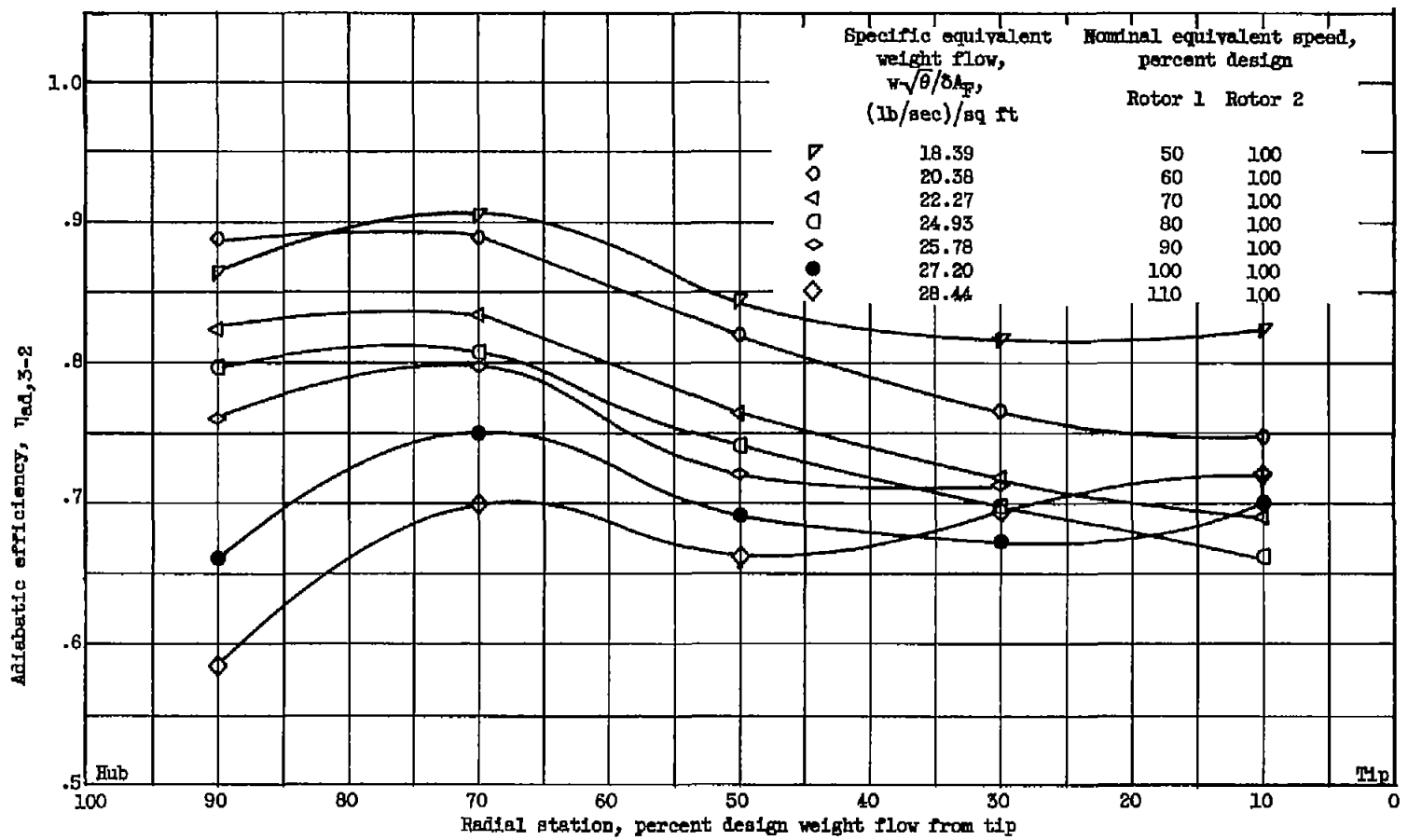

(c) Adiabatic efficiency.

Figure 8. - Concluded. Radial variation of second-stage performance.

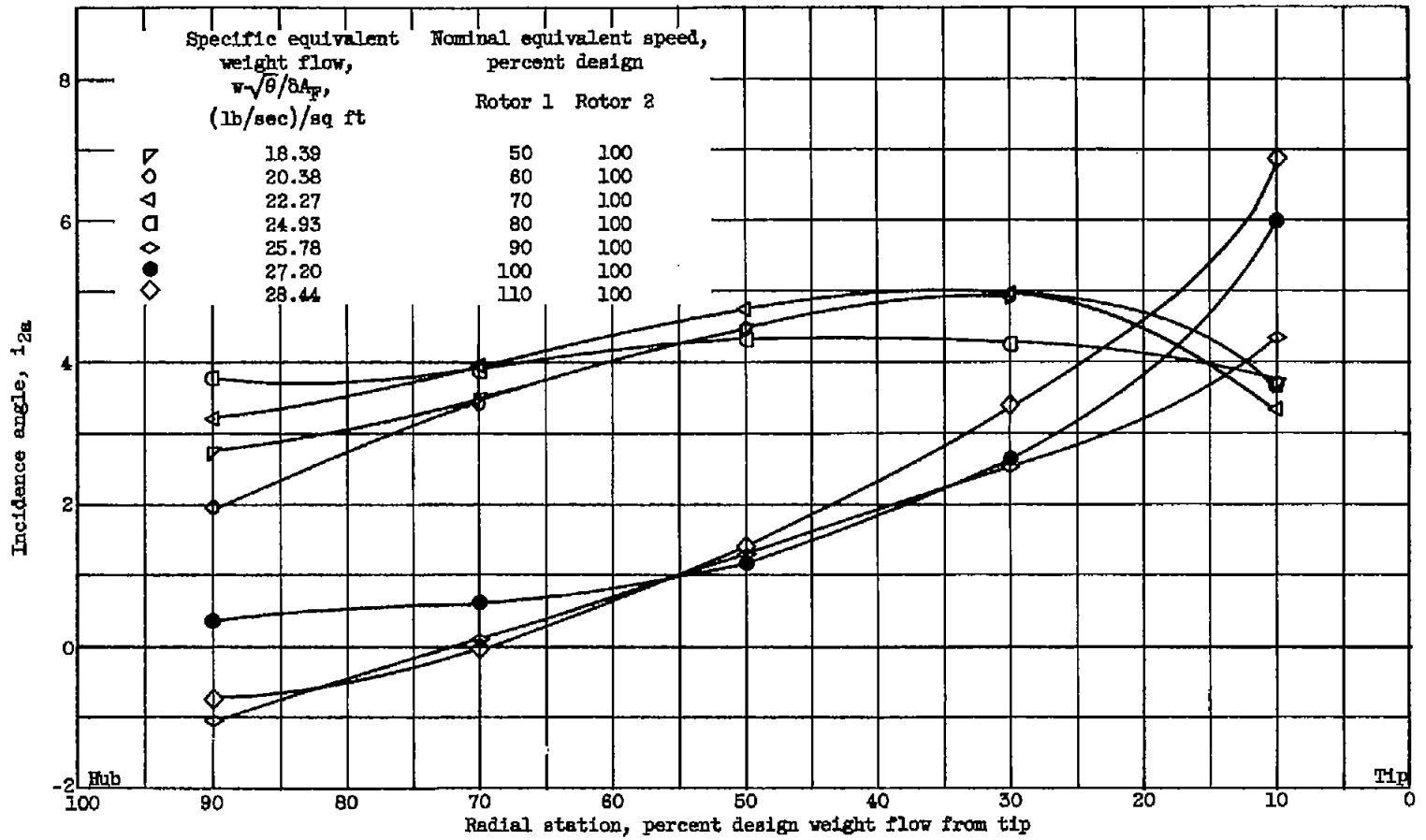

(a) Incidence angle.

Figure 9. - Radial variation of flow conditions for second-stage rotor.

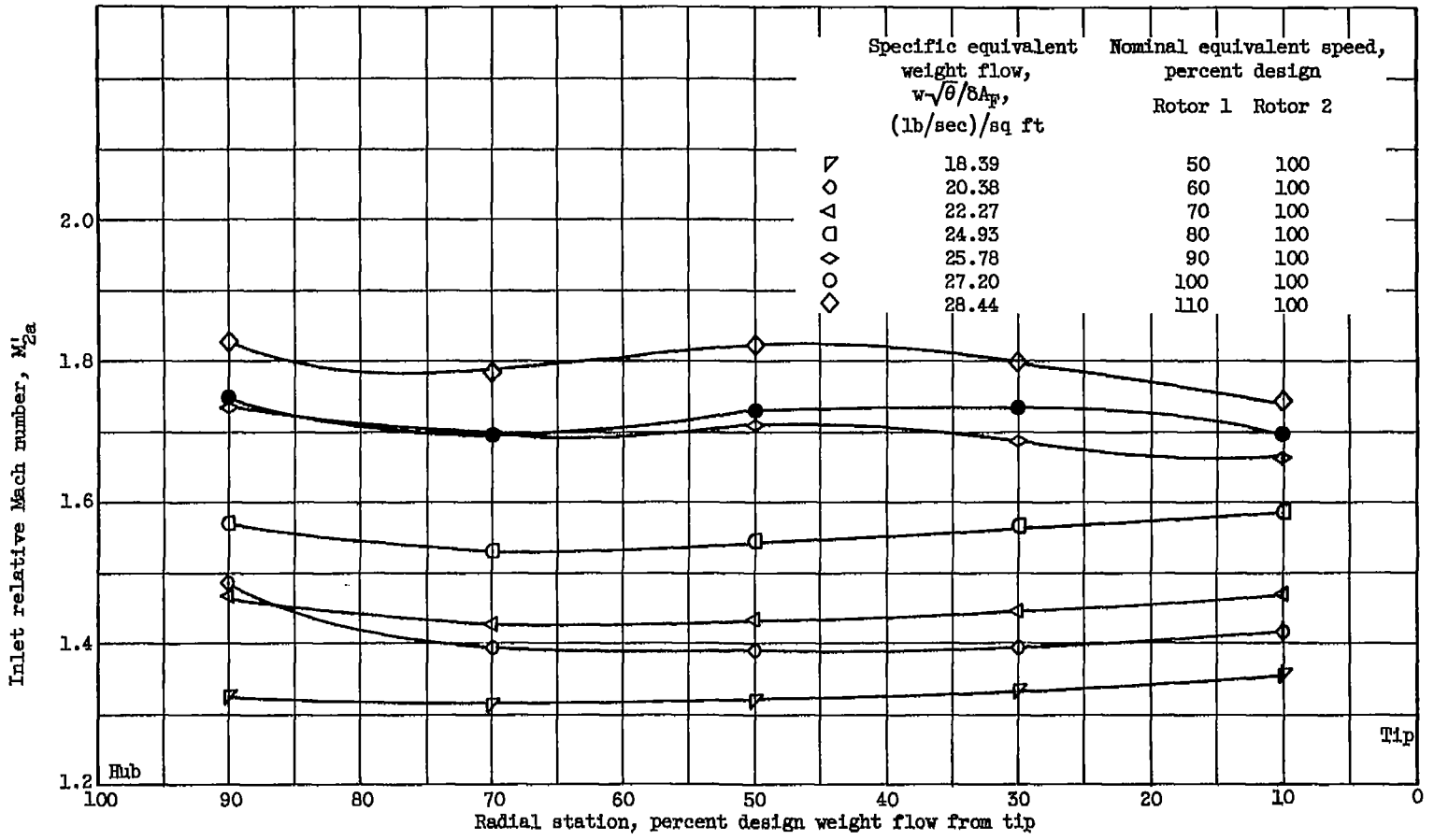

(b) Inlet relative Mach number.

Figure 9. - Continued. Radial variation of flow conditions for second-stage rotor.

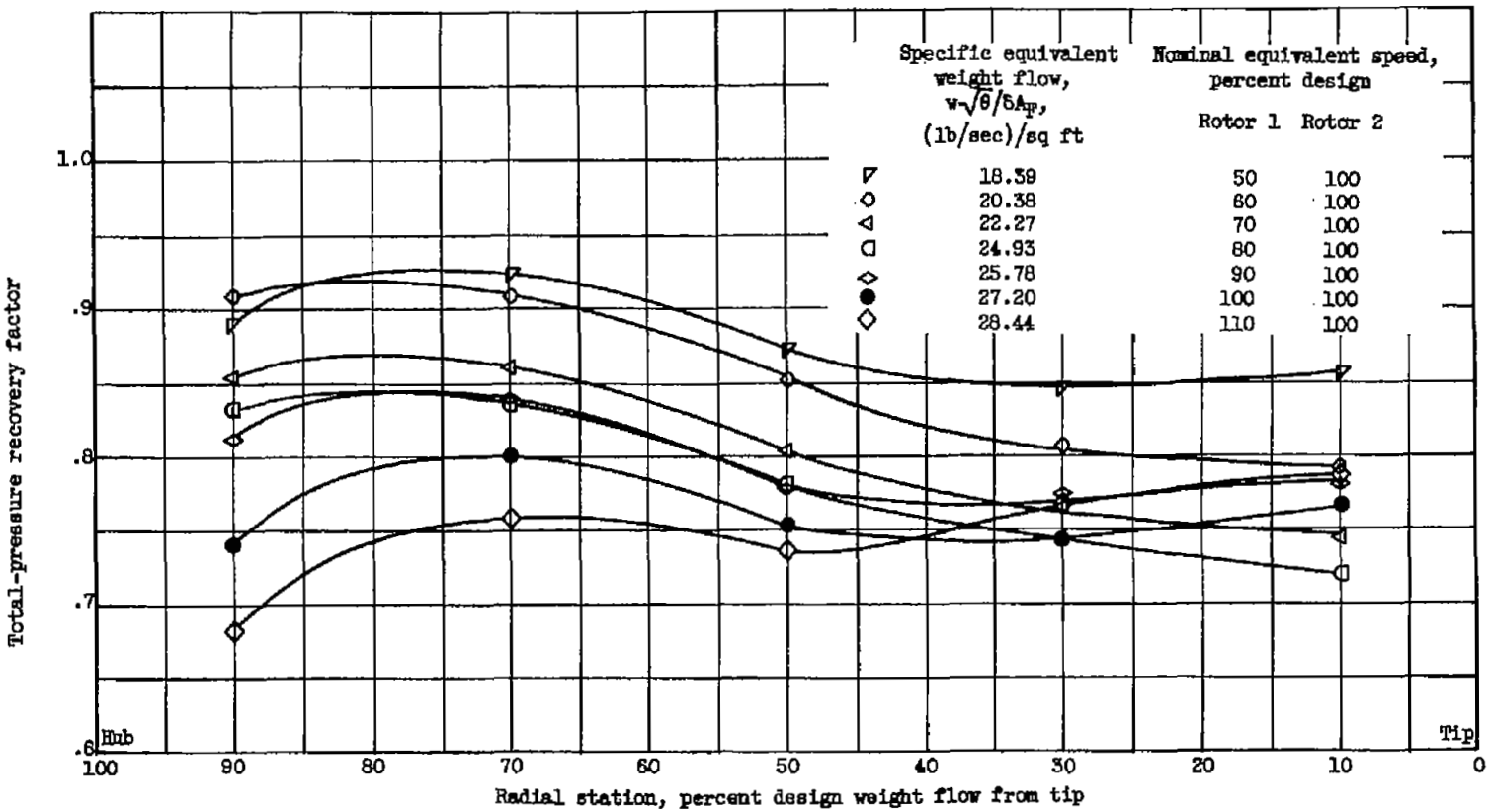

(c) Total-pressure recovery factor.

Figure 9. - Concluded. Radial variation of flow conditions for second-stage rotor.

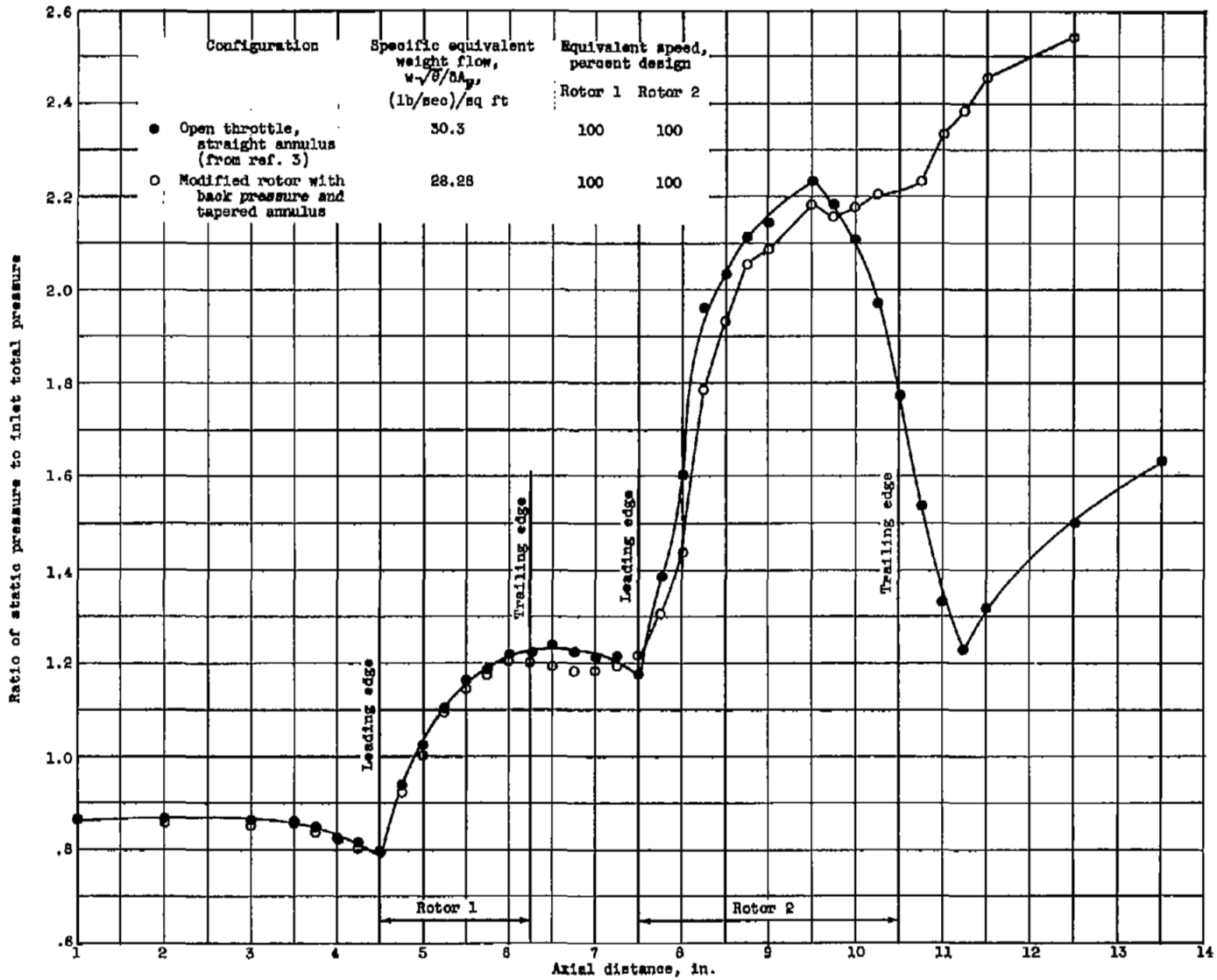

Figure 10. - Static-pressure profiles over both rotors at design speed.

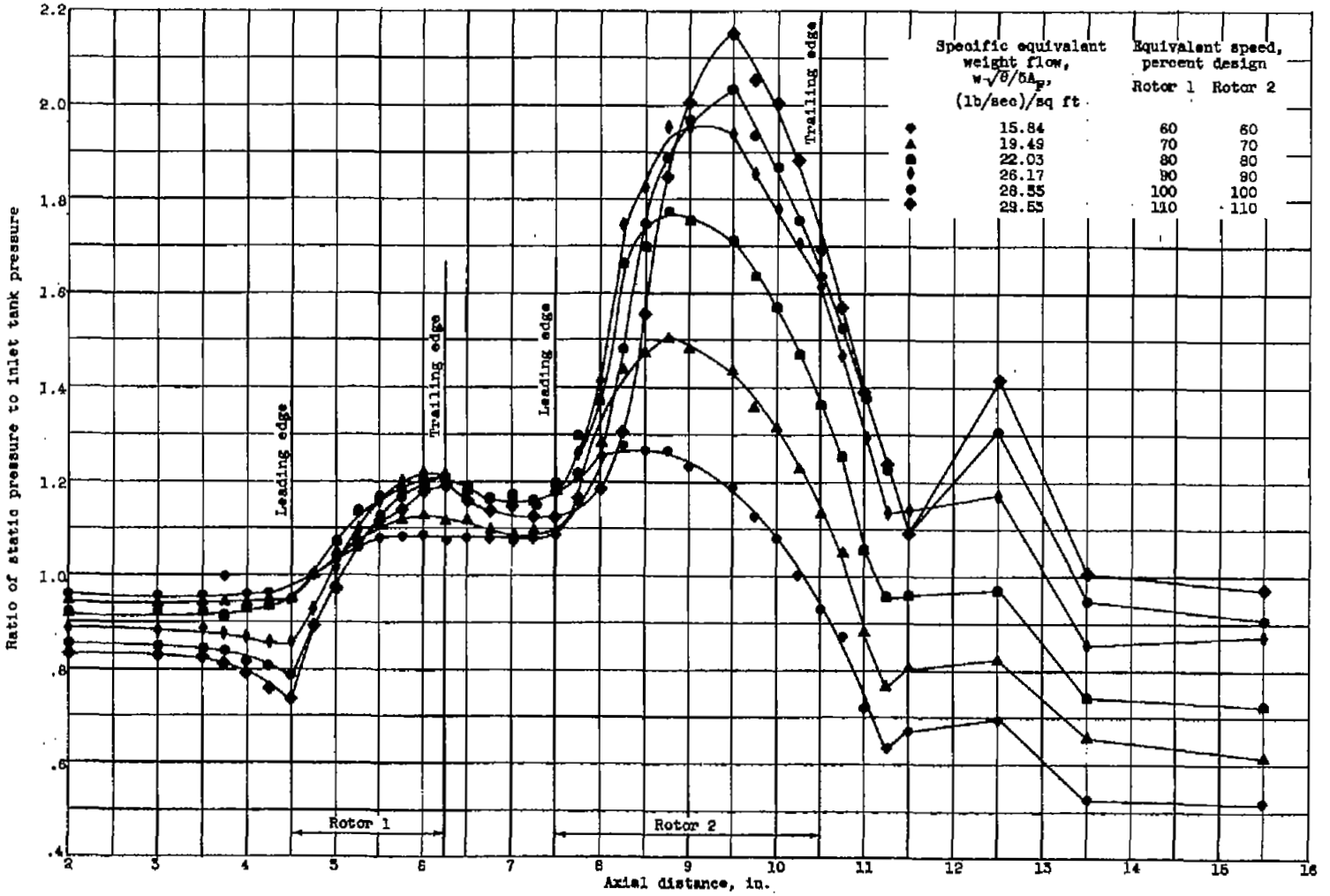

(a) Open-throttle even-speed combinations.

Figure 11. - Static-pressure profiles over both rotors.

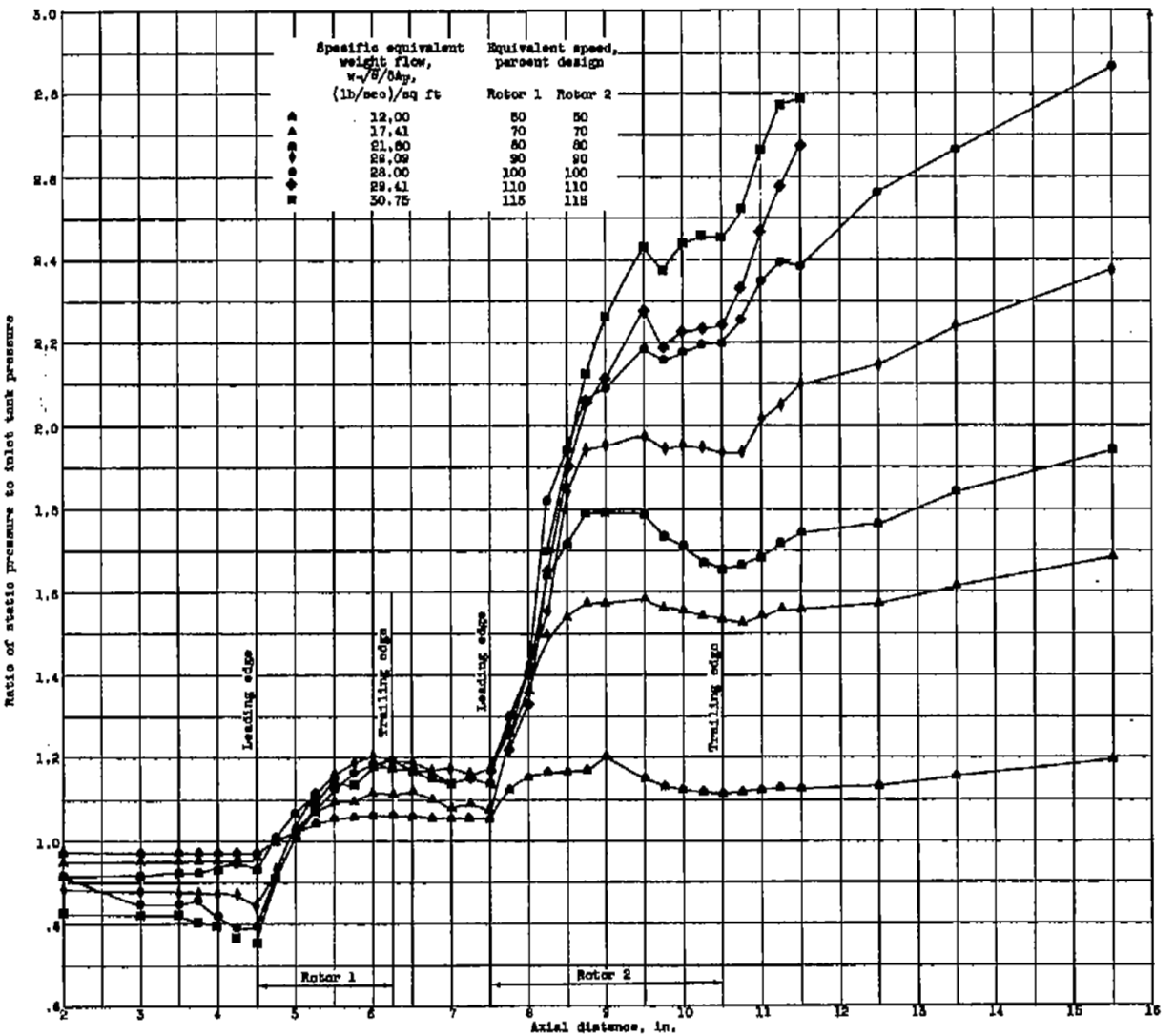

(b) Back-pressure even-speed combinations.

Figure 11. - Concluded. Static-pressure profiles over both rotors.

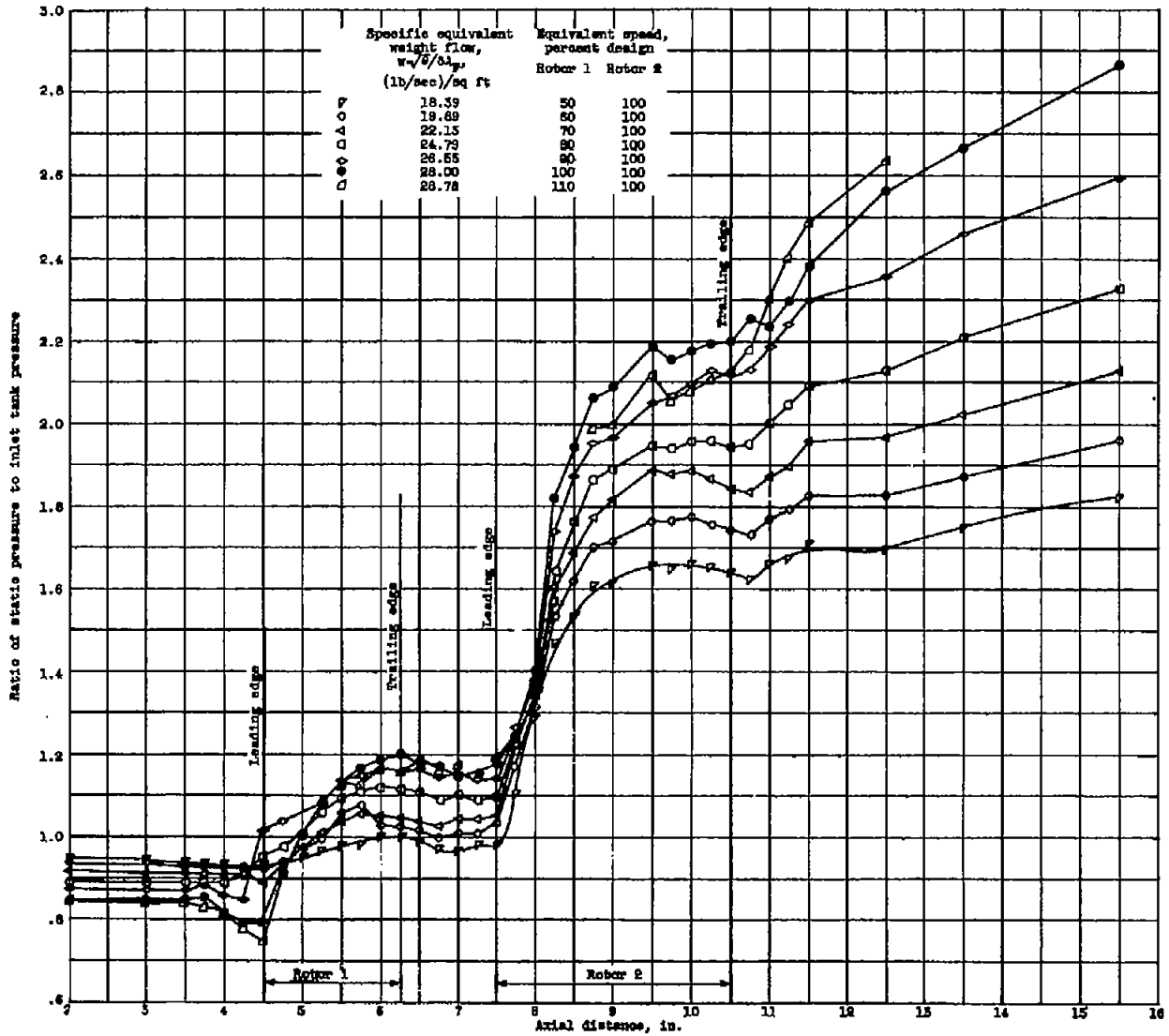

Figure 12. - Static-pressure profiles over both rotors with back pressure (varying first-stage speed, fixed second-stage speed).

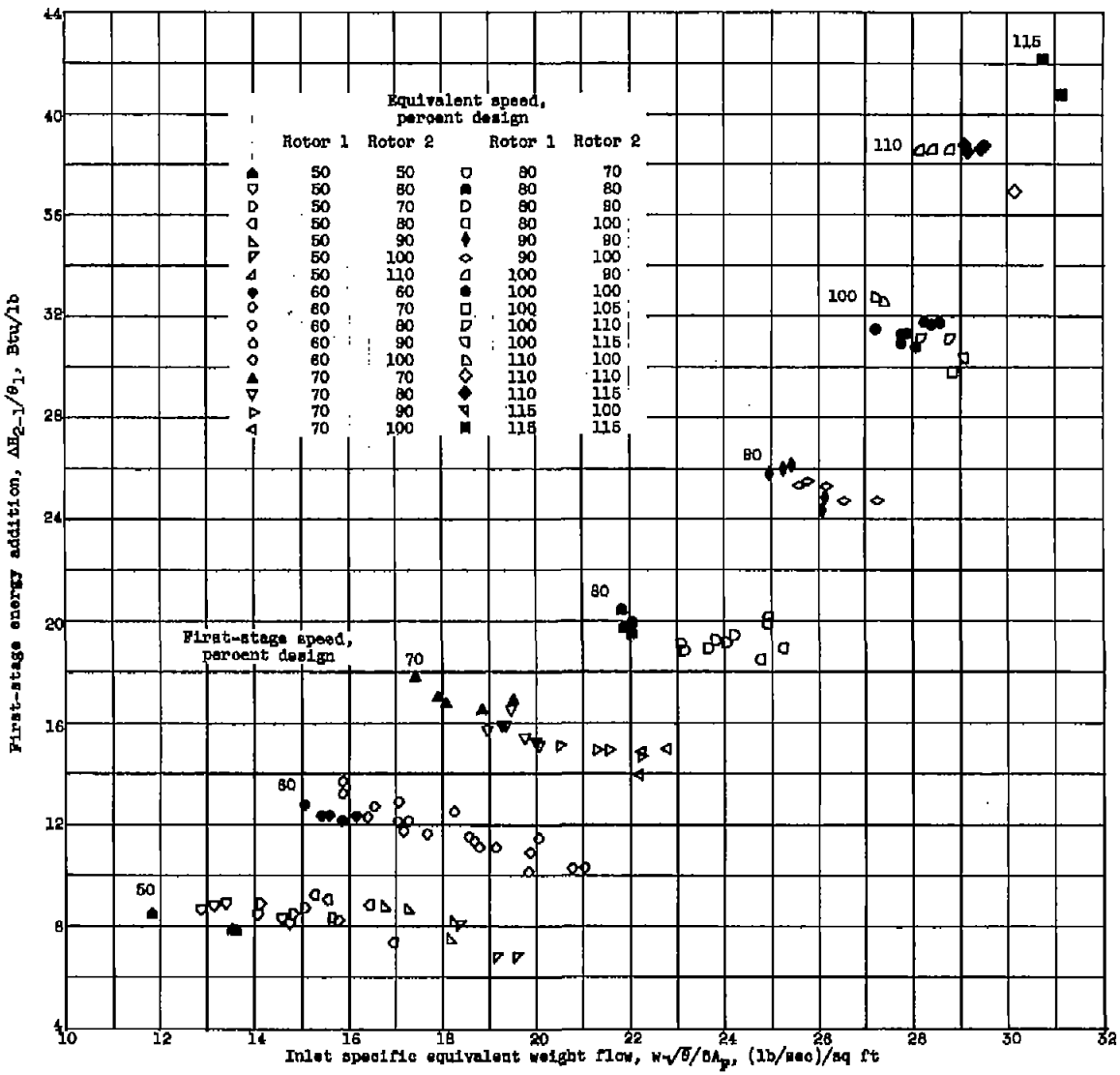

Figure 13. - First-stage energy addition over complete range of conditions tested.

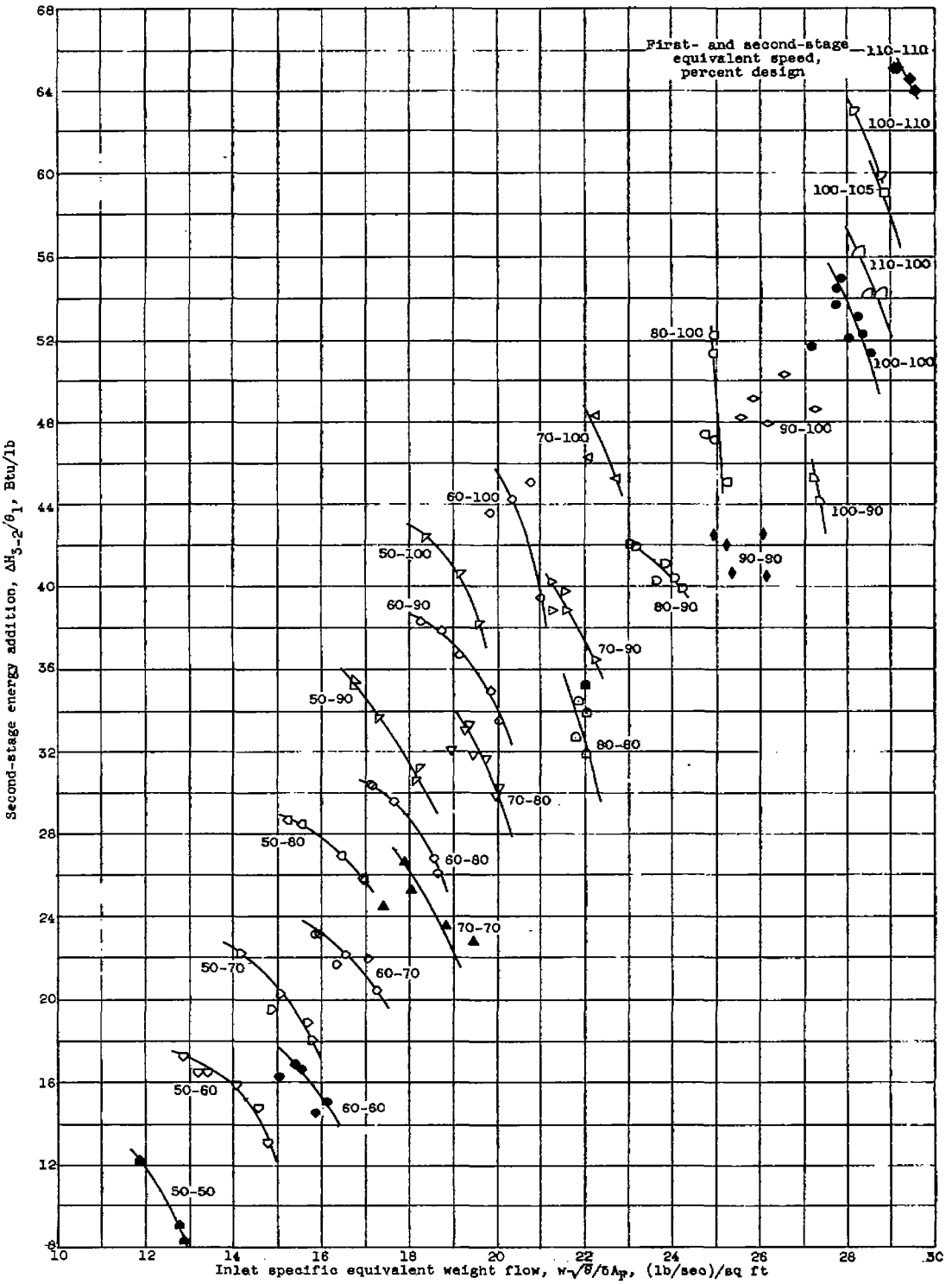

Figure 14. - Second-stage energy addition over complete range of conditions tested.

4655

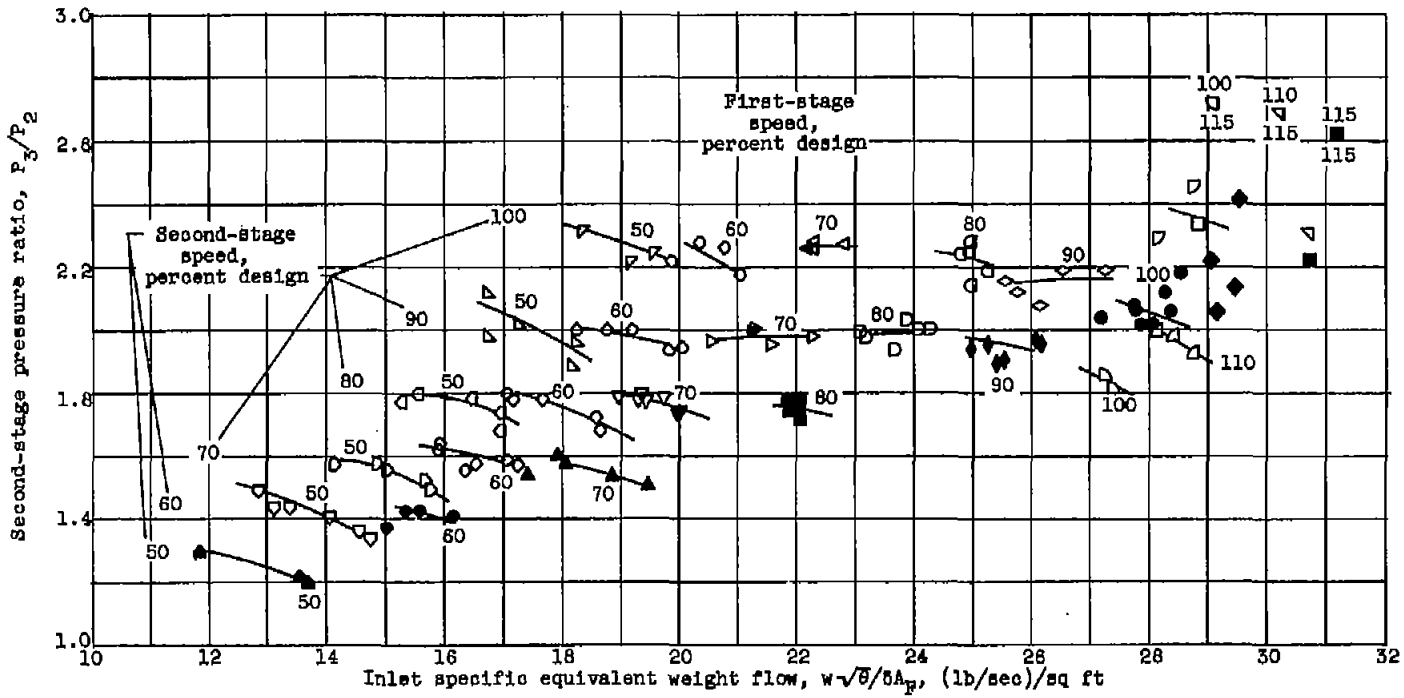

Figure 15. - Second-stage pressure ratio over complete range of conditions tested.